Multilevel diffractive elements for generalized wavefront shaping

Yochay Danziger
Erez Hasman, MEMBER SPIE
Asher A. Friesem, MEMBER SPIE
Adolf W. Lohmann
Weizmann Institute of Science
Department of Physics of Complex Systems
Rehovot 76100, Israel
E-mail: feyochay@wicc.weizmann.ac.il

Abstract. A new approach to designing computer-generated multilevel diffractive elements, in which the phase and the amplitude of the output wavefront can be controlled independently, is presented. In this approach the diffraction efficiency of the elements can be arbitrarily controlled to reach 100% efficiency over the entire element. The approach is based on varying the local diffraction efficiency by changing the width and the number of levels in every period. To reduce complexity, an algorithm for designing the element with the least number of levels and masks is developed. This design algorithm determines the needed mask parameters in which compensation for distortions introduced by the lithographic recording of the element are taken into account. Calculated and experimental investigations that confirm the new design approach are presented.

Subject terms: diffractive optics; diffraction efficiency; computer-generated holograms; diffractive optical elements; multilevel diffractive elements.

Paper 17105 received Oct. 18, 1995; revised manuscript received Feb. 14, 1996; accepted for publication Feb. 15, 1996.

1 Introduction

Computer-generated diffractive optical elements (DOEs) can be formed so they behave as very sophisticated optical elements.[1] For practical optical systems, the DOEs must have high diffraction efficiency. The high efficiency can be obtained by resorting to phase rather than absorptive DOEs, where the phase DOEs are recorded as an etched relief pattern on a substrate. The recording can be performed by means of lithographic techniques, which are used in microelectronics. When coating the relief pattern with a reflective metallic layer, a reflective phase DOE is obtained. When the relief pattern is in a transparent material, a transmittive phase DOE is obtained.

In 1967 Jordan et al.[2,3] suggested blazed relief patterns, namely kinoforms, to obtain 100% diffraction efficiencies. The relief height of the kinoforms are proportional to phase residues after modulo 2π, so their phase variations range from 0 to 2π. Unfortunately, it is difficult to directly record general kinoforms having variable periods and properly shaped blazed grooves. Consequently, in practice, it is necessary to approximate the ideal blazed shape of the grooves with multilevel discrete binary phase levels.[4] The diffraction efficiency of such approximated kinoforms depends on the shape and the height of every level, where for best efficiency the level height must be varied according to the period of the grating and the angle of the incident beam.[5] For DOEs having differing periods, e.g., high-numerical-aperture diffractive lenses, it is not possible to arbitrarily change the height of the individual level, because they are etched simultaneously all over the entire element. Consequently, the overall diffraction efficiency for such DOEs is relatively low. Moreover, by utilizing conventional design methods, it is difficult to independently vary the phase and the amplitude of the output wavefront, as is sometimes necessary for some applications such as matched filtering and subdiffraction limited focusing lenses.[6]

To obtain independent control of the phase and the amplitude, it is possible to exploit a combination of two elements, one of which controls the phase and the other the amplitude.[7] Such a combination, however, requires difficult alignment and recording techniques. Alternatively, two phase-only elements can be used to obtain independent control of the phase and the amplitude of a wavefront by a method called optical coordinate transformation.[8] This method achieves high efficiency, but again requires difficult alignment and necessitates a relatively large distance between the two phase elements. Thus, single DOEs, with phase-only functions, are generally used to approximate those with the required complex functions.[9] Other solutions, developed by Brown and Lohmann[10] and Lee[1] involve the control of the diffraction efficiency to change the amplitude and the phase of the output wavefront. But this solution is suitable for binary DOEs only, where the diffraction efficiency cannot exceed 40.5%.

In this work, we present a novel approach for efficiency optimization by changing the number and width of the levels in every period of a single multilevel DOE, and by ensuring that the number of levels needed to record the element is minimized. This approach can be extended to allow for independent variation of the phase and the amplitude distribution of the output wavefront, while at the same time controlling the diffraction efficiency from 0 to 100%. A relation for the diffraction efficiency of multilevel diffractive elements, which takes into account all the limitations imposed by the realization procedure, is derived. This relation is then exploited for obtaining an algorithm that determines relevant parameters of the DOE, such as the number of levels per each period and the height of each level. These parameters are then used for designing the

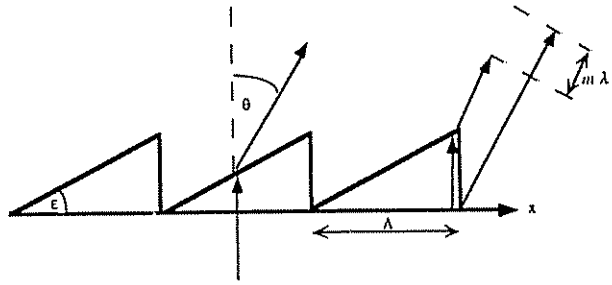

Fig. 1 Profile of a transmission blazed grating

masks that are needed for producing the DOE. The new approach is illustrated by designing and evaluating two different DOEs. In one, the improvement of diffraction efficiency is evaluated with computer simulations. In the other, a multilevel DOE is designed and recorded, and then experimentally evaluated to show independent control of the phase and the amplitude of the output wavefront.

2 Multilevel DOEs—Theoretical Considerations

We present blazed and multilevel DOEs and derive the diffraction efficiency relations for these under certain relevant conditions. These relations are applicable to both transmission and reflection DOEs.

2.1 *Basic Considerations*

We begin by considering a conventional blazed DOE, as shown in Fig. 1. The incident beam is both refracted and diffracted by the DOE at an angle of θ. When the angle of each periodic tooth is ϵ, assuming normal incidence and a surrounding medium of unit refractive index, then the refraction relation can be written as

$$n \sin(\epsilon) = \sin(\epsilon + \theta_r), \tag{1}$$

where θ_r is the refraction angle corresponding to θ in Fig. 1. The diffraction relation is

$$\sin(\theta_d) = \frac{m\lambda}{\Lambda}, \tag{2}$$

where m is the diffraction order and θ_d is the diffraction angle corresponding to θ in Fig. 1. Now, when θ_r in Eq. (1) is the same as θ_d in Eq. (2), i.e., $\theta_d = \theta_r = \theta$, then the diffraction efficiency for the m'th order will be 100%. In such a case, the path difference of rays from the corners of the vertical edge of each tooth is an integer multiple of the wavelength, $m\lambda$.

The diffraction efficiency of the blazed DOE can be controlled by tilting the profile of some of the DOE teeth, as shown in Fig. 2. A regular blazed tooth can produce 100% diffraction efficiency in accordance with scalar approximation.[4] Any tilt of the profile will reduce the efficiency. This is because the tooth angle ϵ is changed, so the condition of θ_d being equal to θ_r is no longer fulfilled. Modification of the phase and the amplitude of the light can be achieved independently by varying the period of the grating Λ for phase changes and the tilt angle of the tooth profile ϵ for amplitude changes. When the tilt pivots around the center of a tooth profile, as shown with tooth profile (b) in Fig. 2, there will only be amplitude changes but no phase change. However, when the tilt pivots around the edge of the tooth profile, as shown with profile (c), the amplitude change is accompanied with some undesirable phase change. This phase change occurs because the average height of the teeth profile changes when pivoting around the edge rather then around the center. This phase change can be compensated for.

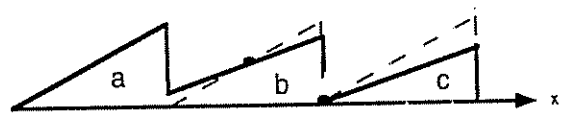

Fig. 2 Profile of blazed DOE having different tilts for each tooth: (a) regular, (b) tilt around the center, and (c) tilt around the edge.

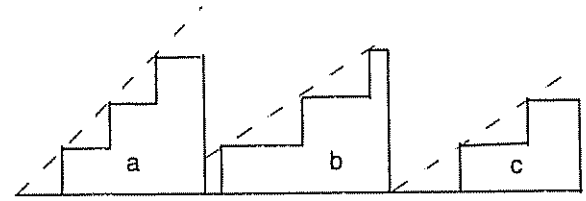

Fig. 3 Four-level approximations of blazed grooves corresponding to Fig. 2: (a) regular, (b) tilt around the center, and (c) tilt around the edge.

In practice, it is difficult to fabricate DOEs with blazed profiles. Consequently, such profiles are approximated by multilevel profiles, as shown in Fig. 3. Here are shown three different quantized (multilevel) blazed teeth corresponding to those shown in Fig. 2. The configuration presented in Fig. 3, profile (c), is more convenient to realize than the one presented in Fig. 3, profile (b), because it requires less levels in every period and the width of the levels is larger, which results with less complication during the realization procedure. In the following, we consider the multilevel DOE in more detail.

2.2 *Diffraction Efficiency Relations*

We now derive the relation of the diffraction efficiency of general multilevel DOEs. Representative multilevel tooth geometry for such DOEs is shown in Fig. 4. The local period is Λ; the height of each level is h; and the local modulation depth (overall height of teeth) is d, running from zero (no levels) to an optimized height d_{opt}, which gives 100% diffraction efficiency.[4] The angular orientation of the incident wave is θ_i and that of the diffracted wave is θ_o.

Rather than start from the wave equations, we begin with the results that were obtained for a general dielectric relief grating,[11] where the amplitude T_m of the wave, in the m'th diffracted order, can be written as

$$T_m = \frac{1}{\Lambda}\int_0^{\Lambda} \exp\left\{-i2\pi\left[\frac{m}{\Lambda} + \frac{f(x)}{\lambda} \times (n_1 \cos\theta_i - n_2 \cos\theta_o)\right]\right\} dx. \tag{3}$$

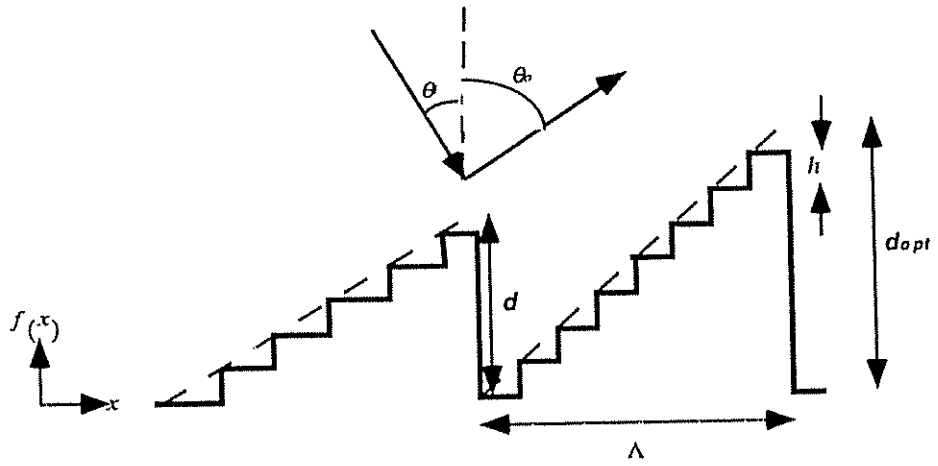

Fig. 4 Geometry of the multilevel DOE. The local number of levels varies according to the local modulation depth d, which range between zero (no levels) to d_{opt}.

In Eq. (3), $f(x)$ is the depth profile, x is the lateral coordinate, n_1 is the refractive index of the surrounding medium, and n_2 is the refractive index of the grating medium; for a reflective grating $n_1=-n_2$. The diffraction angle θ_o is found from

$$\sin\,\theta_o=\frac{\lambda m}{\Lambda}+\sin\,\theta_i. \tag{4}$$

We now introduce the multilevel quantized function into Eq. (3), where the multilevel function is approximated with teeth having the form of the tooth in profile (c) in Fig. 3. The resulting amplitude of the diffracted wave now becomes

$$T_m=\frac{1}{\Lambda}\sum_{p=0}^{p_{\max}-1}\int_{(\Lambda/\xi)p}^{\Lambda/\xi(p+1)}\exp\left[-i2\pi\left(\frac{m}{\Lambda}x+\frac{h}{d_{opt}}p\right)\right]dx + \int_{(\Lambda/\xi)p_{\max}}^{\Lambda}\exp\left[-i2\pi\left(\frac{m}{\Lambda}x+\frac{h}{d_{opt}}p_{\max}\right)\right]dx. \tag{5}$$

In Eq. (5), the optimal modulation depth is the height of the tooth shown in Fig. 4, d_{opt} is

$$d_{opt}=\frac{\lambda}{n_1\cos\,(\theta_i)-n_2\cos\,(\theta_o)}, \tag{6}$$

the local number of levels ξ is the height of each tooth divided by the height of the levels, written as

$$\xi=\frac{d}{h}, \tag{7}$$

and $p_{\max}$ is the number of complete levels in every period

$$p_{\max}=\text{integer}\{\xi\}. \tag{8}$$

For example, in Fig. 4, $p_{\max}=5$ for the smaller tooth and $p_{\max}=\xi=8$ for the large tooth, where $d=d_{opt}$.

The first term in Eq. (5) represents the amplitude of the diffracted wave that is contributed by the complete levels in every period, whereas the second term represents the amplitude that is contributed by the last incomplete level.

The exact solution of Eq. (5) yields the diffraction efficiency, assuming a unit amplitude incident beam, as

$$\eta_m=|T_m|^2=\left|\frac{1}{2\pi m}\left(\left[\exp\left(-i2\pi\frac{m}{\xi}\right)-1\right]\times\frac{1-\exp\,[-i2\pi(\delta/\xi)p_{\max}]}{1-\exp\,[-i2\pi(\delta/\xi)]}+\left\{\exp\left[-i2\pi\times\frac{m}{\xi}(\xi-p_{\max})\right]-1\right\}\exp\left(\frac{\delta}{\xi}p_{\max}\right)\right)\right|^2, \tag{9}$$

where the relative modulation variation is

$$\delta=m-\frac{d}{d_{opt}}. \tag{10}$$

For a small level height, i.e., $h/d_{opt}\ll 1$, we can replace $p_{\max}$ by ξ, so Eq. (9) can be simplified to

$$\eta_m=\left|\left[\exp\left(-i2\pi\frac{m}{\xi}\right)-1\right]\frac{1-\exp\,(-i2\pi\delta)}{1-\exp[-i2\pi(\delta/\xi)]}\right|^2 =\left[\frac{\sin\,(\pi m/\xi)\sin(\pi\delta)}{\pi m\sin\,(\pi\delta/\xi)}\right]^2|\exp\,(-i\pi\delta)|^2. \tag{11}$$

Equation (11) is an exact solution when the modulation depth d is the complete sum of a number of level heights.[4] If we use, for example, a maximum of 16 levels for every tooth of the DOE, then the diffraction efficiency given by the simplified solution of Eq. (11) is within less than 1% from that given by the exact solution of Eq. (9).

With a DOE in which the teeth pivot around the edge rather than the center of each tooth, there is a phase shift in the diffracted wavefront. This shift is evident in the last

term of Eq. (11). Specifically, when $d=d_{\text{opt}}$ is used as a reference, then an approximated phase shift of the diffracted wavefront can be written as

$$\Delta\phi=\phi_{d_{\text{opt}}}-\phi_d=\delta\pi, \tag{12}$$

where δ is the relative modulation variation. Alternatively, an exact phase shift can be derived numerically from Eq. (9), with the result being comparable to that of Eq. (12). When designing DOEs, it is necessary to eliminate such a phase shift. This is done by modifying the desired phase ϕ_{desired} to obtain a modified phase ϕ_{modified}, in accordance to

$$\phi_{\text{modified}}=\phi_{\text{desired}}-\Delta\phi. \tag{13}$$

It is possible[5] to determine the optimal depth of modulation that would maximize the diffraction efficiency for an entire range of incidence angles and wavelengths, by maximizing the overall diffraction efficiency $E(d)$. This overall diffraction efficiency can be written as

$$E(d)=\int\int \omega(\theta_i,\lambda)\,\eta(\theta_i,\lambda,d)\,\mathrm{d}\theta\,\mathrm{d}\lambda, \tag{14}$$

where $\omega(\theta_i,\lambda)$ is the angular and spectral energy distribution of the incident light and $\eta(\theta_i,\lambda)$ is the diffraction efficiency given by Eq. (11). When the period of the DOE is small, i.e., $\Lambda\approx\lambda$, then $\eta(\theta_i,\lambda)$ should be calculated by resorting to vectorial calculations.

To obtain an undistorted diffracted wavefront, it is necessary to ensure that all higher orders do not overlap on the desired (first) order. This can be readily achieved by introducing a sufficient linear phase to the desired phase of the diffracted wavefront, so it will be angularly separated from the other orders.[12] Finally, since in practice h is constant, the diffraction efficiency, given by either Eq. (9) or Eq. (11), is essentially a function of d only, i.e., $\eta_m[d(x,y)]$. Thus, by changing d it is possible to control and optimize the diffracted efficiency.

2.3 *Comparison with Conventional Design Method*

It is useful to compare DOEs where profiles are formed in accordance with our optimization method with those formed with conventional methods. The basis for comparison will be how high a diffraction efficiency can be achieved with any of the methods. For this comparison, we consider a reflective focusing DOE that operates with an off-axis angle to separate the incident and the diffracted waves. The geometry of such a DOE with the participating wavefronts is shown in Fig. 5. The incident beam is a plane wave oriented at an angle θ_i with respect to the normal. The diffracted output wavefront converges to a point, with the central ray oriented at an angle θ_o to the normal.

With conventional designs where the modulation depth is constant over the entire DOE, the modulation depth variation of the first diffracted order can be derived in accordance with Eqs. (6) and (10) as

$$\delta=1-\frac{d}{d_{\text{opt}}}=1-\frac{\cos(\theta_i)+\cos(\theta_o+\Delta\theta)}{\cos(\theta_i)+\cos(\theta_o)}, \tag{15}$$

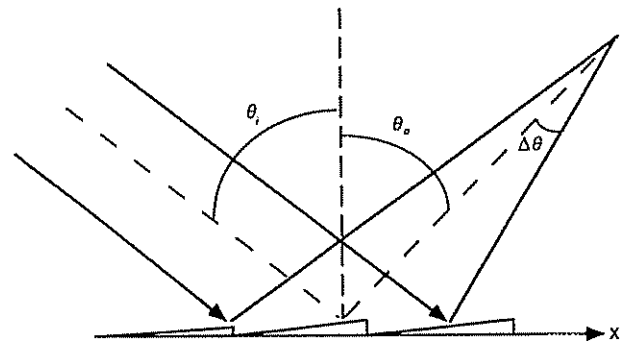

Fig. 5 Geometry of reflecting focusing DOE.

where θ_i is the incidence beam angle, θ_o is the diffracted beam angle, and for simplification we consider the diffracted angle at the edge as $\theta_o+\Delta\theta$. Here d_{opt} is the optimal modulation depth for θ_i and θ_o. For $\theta=\theta_i=\theta_o$ and assuming paraxial conditions, Eq. (15) can be simplified to

$$\delta=\tfrac{1}{2}\tan(\theta)\ \sin(\Delta\theta). \tag{16}$$

Equation (16) indicates that the modulation depth variation δ increases as the incidence and diffraction angles become larger and as the numerical aperture becomes larger (numerical aperture is proportional to $\Delta\theta$). This implies that the diffraction efficiency will decrease rapidly. As an example, consider a focusing element with $f/\#=1.5$, a maximum of 16 levels in every period, and $\theta=45$ deg. For these parameters the modulation depth error is 15% at the edge, with a corresponding reduction of diffraction efficiency by 8%. With our method, on the other hand, the modulation depth variation δ is zero, but the number of levels in each period is altered. When the same parameters of the preceding example are introduced into Eq. (9), the resulting reduction in diffraction efficiency is only 0.5%.

The diffraction efficiency as a function of the lateral coordinate along a reflective focusing DOE is shown in Fig. 6. The results are for DOEs that are formed in accordance with conventional methods and those that are formed by our optimized method. The parameters were the same as those used in the example before, except that $\theta=40$ deg for one DOE and $\theta=50$ deg for the other. As is evident, the diffraction efficiency reduction for the DOEs formed conventionally is significantly greater than the corresponding DOEs formed in accordance with our optimization method. The height of every level was kept constant in every element and was equal to the largest modulation depth in the element divided by 16. Note that if the number of levels were greater than 16, the reduction of diffraction efficiency for the optimized DOE will be even smaller, while at the same time no significant efficiency change in the conventional elements will occur.

3 Design Procedure

In the fabrication of the multilevel DOEs, several computer-generated masks are exploited. We describe how these masks are designed.

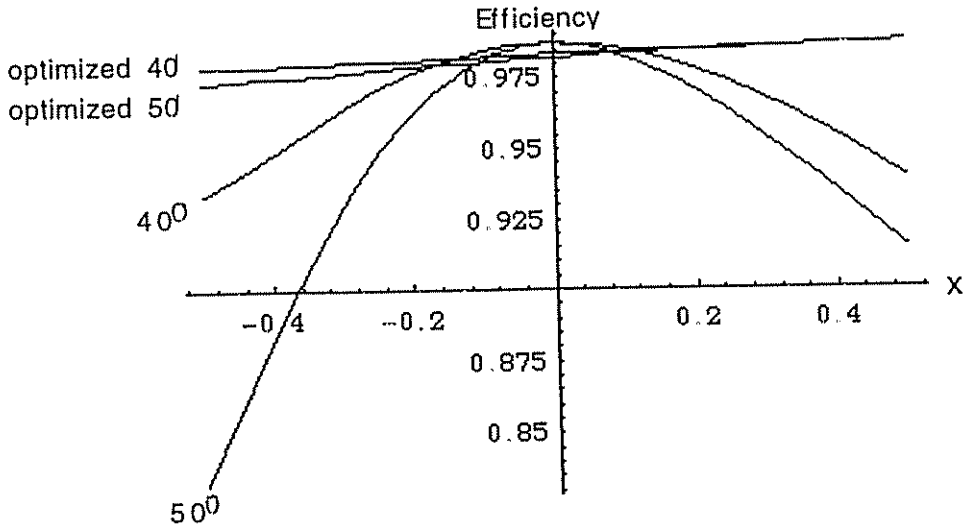

Fig. 6 Diffraction efficiency as a function of distance from center of conventional and optimized reflecting focusing DOEs at incidence angles of 40 and 50 deg.

3.1 *Design Parameters*

In multilevel DOEs, it is best to minimize the number of levels, but still retain the high diffraction efficiencies. Such minimization results in decreasing the fabrication errors and thereby reduce the scatter noise, as well as in simplifying the recording procedure. To determine the parameters of the masks that are needed to fabricate a DOE with a minimum number of levels, we begin with Eq. (11). When the number of levels in each period does not depend on the relative modulation variation [i.e., $\xi(\delta)=\text{const}$], then the maximal efficiency in Eq. (11) occurs at $\delta(x,y)=0$. Thus, $d=d_{\text{opt}}$. Letting the height h of each level be a free parameter, Eq. (11) simplifies to

$$\eta_1(x,y)=\left[\frac{\sin\ (\pi/N')}{\pi/N'}\right]^2, \tag{17}$$

where

$$N(x,y)=\xi_{\text{opt}}(x,y)=\frac{d_{\text{opt}}(x,y)}{h(x,y)}. \tag{18}$$

For any desired $\eta_1(x,y)$ and a certain d_{opt} [see Eq. (6)], it is possible to derive from Eq. (17) [or from Eq. (9) for the nonapproximated case] the height $h(x,y)$ of the levels at each location of the DOE. In practice, it is extremely difficult to form DOEs having variable level heights. Consequently, we determine the smallest level height, h_{min}, in the entire DOE, and set all levels in the element to be of that height. At the coordinates of this h_{min}, the desired efficiency η_1 can be achieved. At other locations, $\delta(x,y)$ must be increased to obtain the desired efficiencies there. Of course, it is possible to choose a lower value for h_{min} and still obtain the desired efficiency. But a lower value implies that the number of levels must be increased, and thereby increasing the recording complexity.

Now, by using h_{min}, Eqs. (7) and (10) with Eq. (9) or Eq. (11), we obtain that the diffraction η_m is solely a function of $\xi(x,y)$. We thus choose the highest possible $\xi(x,y)$ for the entire element, and use it to determine the number of masks M_{max} and thereby the highest number of levels that are needed. This is done in accordance to the inequality

$$2^{M_{\text{max}}}=N_0\geqslant\xi_{\text{max}}>2^{M_{\text{max}}-1}, \tag{19}$$

where M_{max} and N_0 are integers, representing the number of masks needed for the element and the maximal number of levels in every period. Finally, the maximal modulation depth d_0, when using M_{max} masks with h_{min} as step height, is found from

$$d_0=N_0h_{\text{min}}. \tag{20}$$

The preceding procedure can be summarized with the following steps:

1. Let $\delta=0$, then from Eq. (17) or Eq. (9), get $h(x,y)$.
2. Find the lowest $h(x,y)$ for the entire element, to get h_{min}.
3. Now, let $\delta\neq0$, $h=h_{\text{min}}$, and $d=h_{\text{min}}\xi$, then from Eq. (9) or Eq. (11), find $\xi(x,y)$.
4. Find the maximum $\xi(x,y)$ for the entire element to get ξ_{max}.
5. Use Eqs. (19) and (20) to find N_0, d_0, and M_{max}.

3.2 *Design of the Masks*

The amplitude transmittance for the M'th mask with constant modulation depth of 2π, can be written as

$$T=t\{\sin\ (k\phi)\}, \tag{21}$$

where ϕ is the phase of the DOE,

$$T=t\{x\}=\begin{cases}1 & \text{for } x>0\\ 0 & \text{for } x\leqslant0\end{cases},$$

and

$k=2^{M-1}$.

The modulation depth can be changed so as to obtain differing diffraction efficiencies by using that phase part of the grating function that remains after removing the modulus of 2π. Specifically, the overall phase of the grating function is

$$\phi=2\pi N_1+R, \tag{22}$$

where N_1 is an integer, and the remainder R is $R=\text{mod}(\phi/2\pi)$. Substituting Eq. (22) into Eq. (21), yields

$$T=t\{\sin\ (k\phi)\}=t\{\sin\ (k2\pi N_1+kR)\}=t\{\sin\ (kR)\}. \tag{23}$$

When the modulation depth d differs from the maximal d_0, it is necessary to modify R in accordance with

$$R\rightarrow R\,\frac{d}{d_0}. \tag{24}$$

Then the transmittance of the M'th mask given by Eq. (23) becomes

$$T=t\left\{\sin\ \left(kR_1\,\frac{d}{d_0}\right)\right\}=t\left\{\sin\ \left[2^{M-1}\ \text{mod}\left(\frac{\phi}{2\pi}\right)\frac{d}{d_0}\right]\right\}. \tag{25}$$

The modification that leads to Eq. (25) introduces distortions to the transmittance T of the mask when $d/d_0\neq 1$. This distortion is readily evident when we consider, for example, a linear grating, and plot the argument of t as a function of the x coordinate before and after modification. Such plots are shown in Fig. 7; for these $x=\phi/2\pi$ and $M=1$. Figure 7(a) depicts the unmodified argument plotted in accordance to Eq. (21) with $d/d_0=1$. Figure 7(b) depicts the modified argument plotted in accordance to Eq. (25) with $d/d_0=0.85$ (chosen arbitrarily). As evident from these plots, the sinusoidal shape is distorted, where the duty cycle q is changed from $q=1/2$ to some modified value.

3.3 *Fabrication Errors and Compensation*

For the fabrication of computer-generated DOEs conventional lithographic techniques are exploited. In our experiments, these involved wet etching of a photoresist layer as well as of a substrate layer to form the desired surface profile. This wet etching typically increases the width at the top of the etched layers and changes the shape from straight edge walls to sloped walls, as illustrated in Fig. 8.

To correct for such an error, which is introduced by the etching, it is best to reduce the width of the etched level by decreasing the open regions in the mask that are used for exposing the photoresist. Mathematically, this can be represented by an increase of the duty cycle, as

$$q_{\text{new}}=q_{\text{old}}+\Delta q=\frac{1}{2}+\frac{\Delta x}{\Lambda}=\frac{1}{2}+\Delta x\,\frac{|\nabla\phi|}{2\pi}, \tag{26}$$

where $|\nabla\phi|=|\partial\phi/\partial x|$, Δx is the width of the error introduced by the first mask ($M=1$), and $q_{\text{oil}}=1/2$ the duty cycle in the original mask. The compensated duty cycle of Eq.

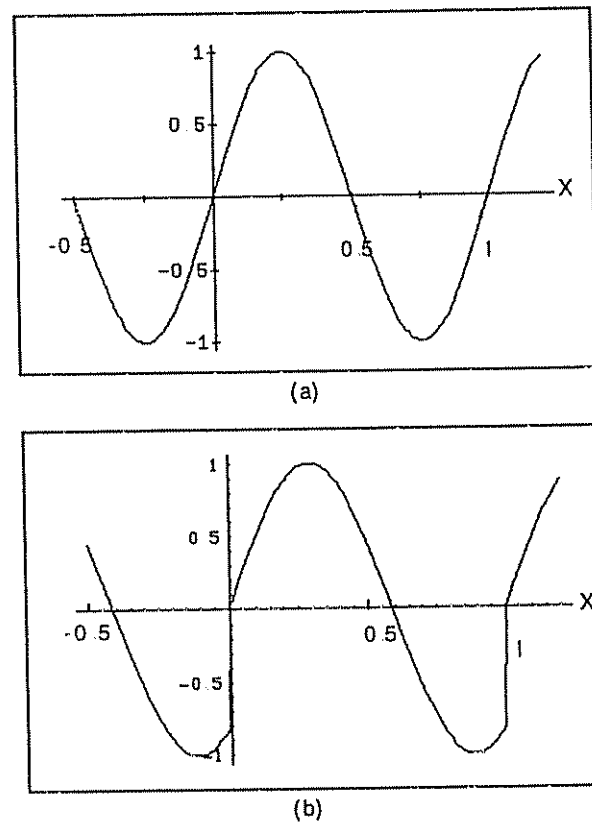

Fig. 7 Argument of t in Eq. (25) as a function of the displacement in DOE with linear phase: (a) unmodified argument $d/d_0=1$ and (b) modified argument $d/d_0=0.85$.

(26) is now introduced into Eq. (25), along with the addition of a bias term $\sin\ [\pi(d/d_0)\Delta q]$. This yields

$$T=t\left\{\sin\ \left(2^{M-1}\,\frac{d}{d_0}\left\{\text{mod}\left[\frac{\phi+(\pi\Delta q/2^{M-1})}{2\pi}\right]-\frac{\pi\Delta q}{2^{M-1}}\right\}\right)+\sin\ \left(\pi\,\frac{d}{d_0}\,\Delta q\right)\right\}, \tag{27}$$

where $\Delta q=\Delta x(|\nabla\phi|/2\pi)$.

Plots of the argument of t in Eq. (27) as a function of x, where $x=\phi/2\pi$, for $M=1$ and $M=2$, are shown in Fig. 9. These plots correspond to that shown in Fig. 7. As is evident, the regions that are used for etching are now narrower.

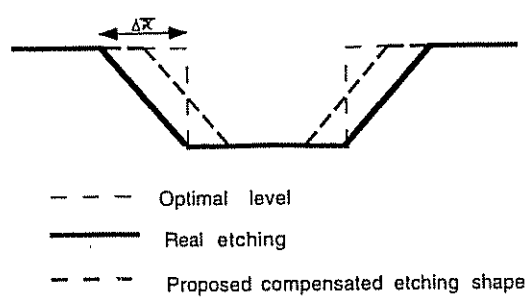

Fig. 8 Wet etching during photolithography introduces distortions.

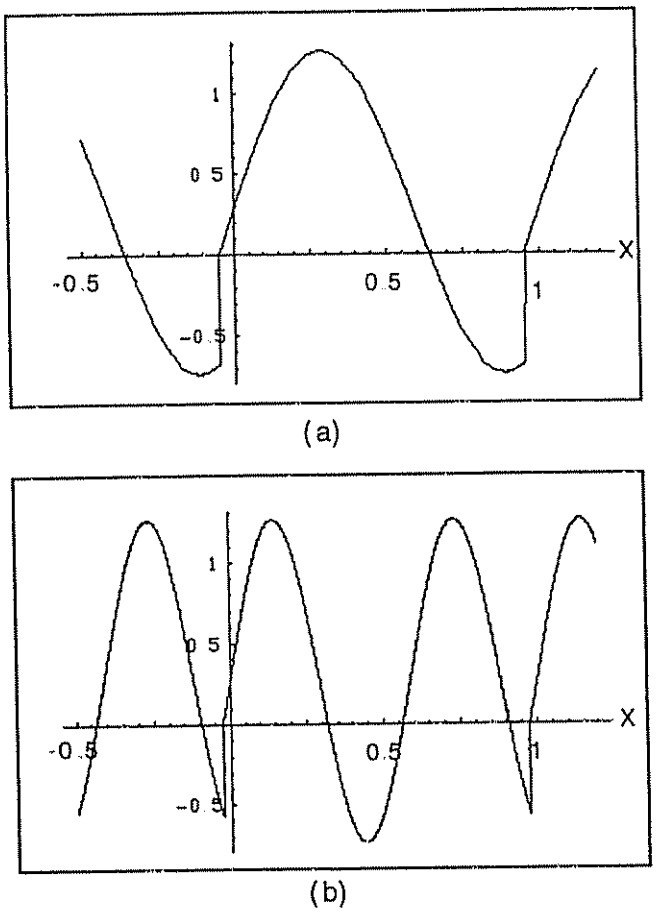

Fig. 9 Argument t in Eq. (27) as a function of displacement with compensation for etching errors: (a) first mask $m=1$ and (b) second mask $m=2$.

4 Experimental Procedure and Results

We illustrate how to independently vary the amplitude and phase of the wavefront that emerges from a DOE. For this illustration, we designed and recorded a cylindrical DOE and then evaluated its performance.

4.1 *Design and Recording of a Cylindrical DOE*

To verify our design method in which we can independently control the amplitude and the phase of the output wavefront, we designed, recorded, and tested a cylindrical DOE. The phase function of this DOE depends on one spatial coordinate only, say, y, and it is so designed to create a cylindrical wavefront that converges to a line along the x axis at the focal plane. The phase function, namely grating function, can be written as

$$\phi=\frac{2\pi}{\lambda}\left[(y^2+F^2)^{1/2}-F\right], \tag{28}$$

where F is the focal length of the DOE. The DOE together with the incident plane wave and converging output wavefront are shown in Fig. 10.

We designed the DOE so that the intensity along the line at the focus increases linearly. To control the intensity of the output wavefront, we first followed the procedure described in Sec. 3.1 to determine the needed level height. Then, we used Eq. (9) to find the modulation depth $d(x,y)$ at every location of the DOE, so as to yield the desired linear intensity distribution. We modified the phase because of changes introduced by the modulation change. Finally, both $\phi(x,y)$ and $d(x,y)$ were substituted into Eq. (27) to obtain the mask transmittance that was used for recording the DOE. To obtain high diffraction efficiency, we used four masks that can result in, at most, 16 levels per each period of the DOE. Representative magnified sections of the central parts in the four masks are shown in Fig. 11. These indicate that the fringes need not be continuous, as is usually for other design methods. Moreover, as we move along the x axis, the element has more levels in every period while the periodicity along the x axis remains.

For the recording of the DOE we exploited conventional lithographic techniques with wet chemical etching for transforming the mask data onto a GaAs substrate. The finest resolution that was obtained with our equipment was about 3 μm. The size of the final DOE was 30×30 mm and its focal length was 240 mm. Figure 12 shows profilometer scans of three different locations of the recorded DOE that have about the same period. As evident, the height of every level is indeed constant regardless of location, while the

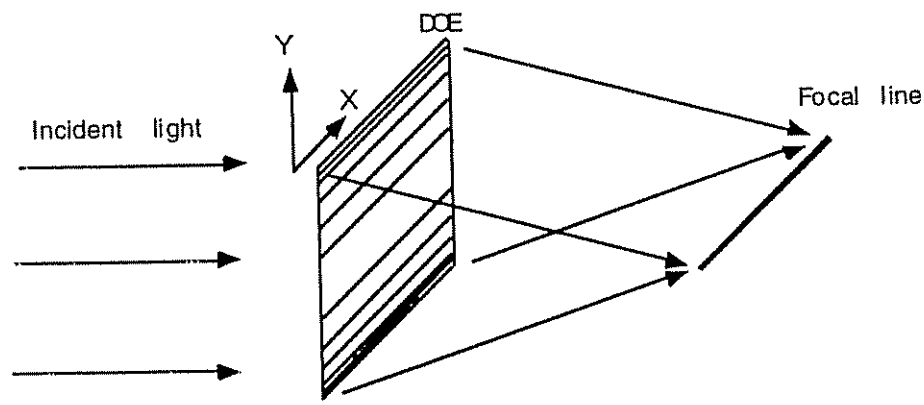

Fig. 10 Geometry of the incident and output wavefronts from a cylindrical DOE.

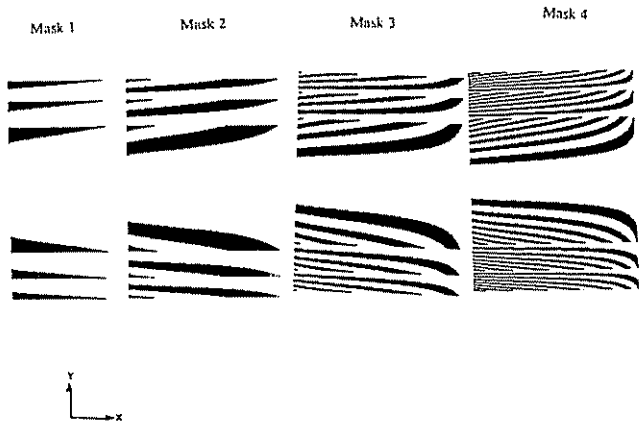

Fig. 11 Central sections of the masks used to fabricate the multilevel DOE.

number of levels is different. The difference in the number of levels arises from the fact that the modulation depth is varied. As shown, the width of the last level in each period may not necessarily be equal to the other level widths, so the number of levels in every period may not be an integer. With each scan in Fig. 12, we also indicate the diffraction efficiency η_1 that was calculated for the specific modulation depth. As expected, the diffraction efficiency increases as the modulation depth becomes longer.

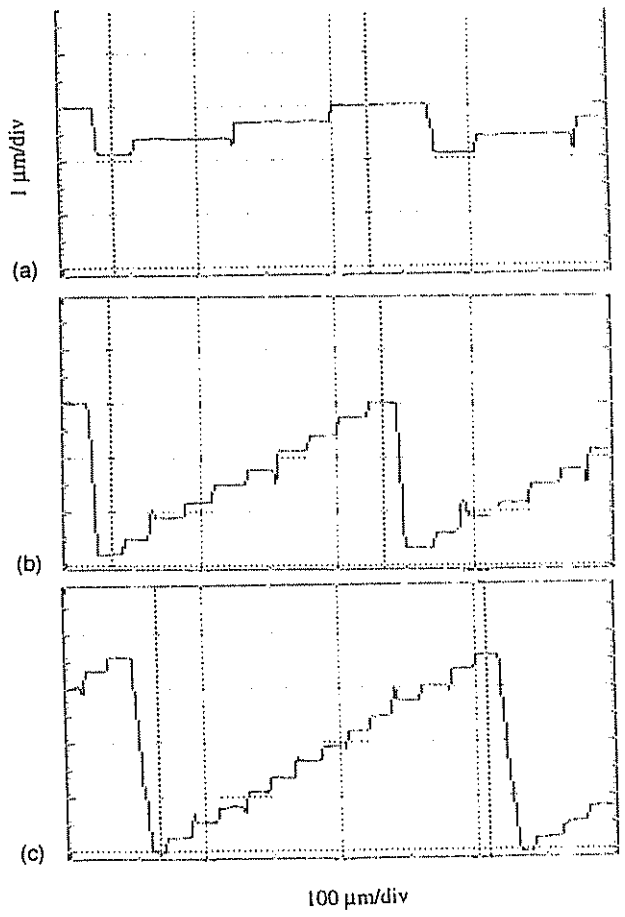

Fig. 12 Profilometer scanning of three different locations of the element, which has the same periodicity. The level height is constant all over the element, while the variation in modulation depth causes variation in local number of levels. The last level (the lower step in every period) is not always complete so the local number of steps is not an integer. (a) Profile 1: number of levels: 3.4; efficiency: 0.06. (b) Profile 2: number of levels: 7.75; efficiency: 0.39. (c) Profile 3: number of levels: 13.6; efficiency: 0.87.

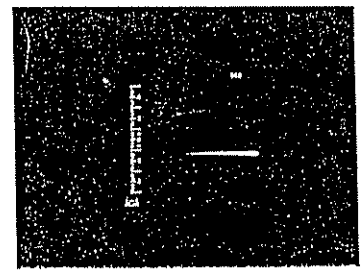

Fig. 13 Thermal imaging of the intensity distribution at the focus

4.2 *Experimental Arrangements and Results*

The experimental arrangement for evaluating the performance of the DOE was comprised of a CO_2 laser, a beam expander and collimator, and a detection system. The light emitted from the CO_2 laser, at 10.6 μm, was expanded and collimated, and the resulting plane wave illuminated the entire DOE. This light converged to a line at the focus of the DOE. At the focal plane we first detected the entire line with a thermal camera. This enabled us to obtain a qualitative measure of the intensity distribution at the focus. To obtain a quantitative measure of the intensity distribution, we added, at the focal plane, a slit that was translated by a stepper motor, and collected the light, that passed through the slit at each location, onto a thermal detector.

The results of these experiments are shown in Figs. 13 and 14. The results for Fig. 13 were obtained with the thermal camera and show the qualitative intensity distribution at the focus. It is interesting to note that the intensities of the other diffraction orders, including the zero order, are very weak and not observable with the thermal camera. Figure 14 shows the quantitative measurements with the scanned slit and thermal detector. As is evident, the intensity distribution along the focus is indeed linear, as expected. Deviation from linearity at the high intensity levels is attributed to diffraction at the edges of the DOE.

We also performed an experiment to measure the power in each of the detectable diffraction orders. These included -1, 0, $+1$, and $+2$ diffraction orders. In this experiment, we used the direct narrow beam from the CO_2 laser (about 1 mm in diameter) to illuminate a small region of the DOE with high intensity. In this way, we could readily separate the various diffracted orders. The illumination beam was moved along the x direction of the DOE, and at every 1-mm displacement we measured the power in each of the relevant diffraction orders.

The predicted and experimental results for the power in four diffraction orders are presented in Figs. 15 and 16. The predicted results, shown in Fig. 15, were calculated in accordance with Eq. (11). As is evident, the powers are mainly in the zero and first diffraction orders. Figure 16 shows the corresponding experimental measurements. As is evident, these are in agreement with the calculated results.

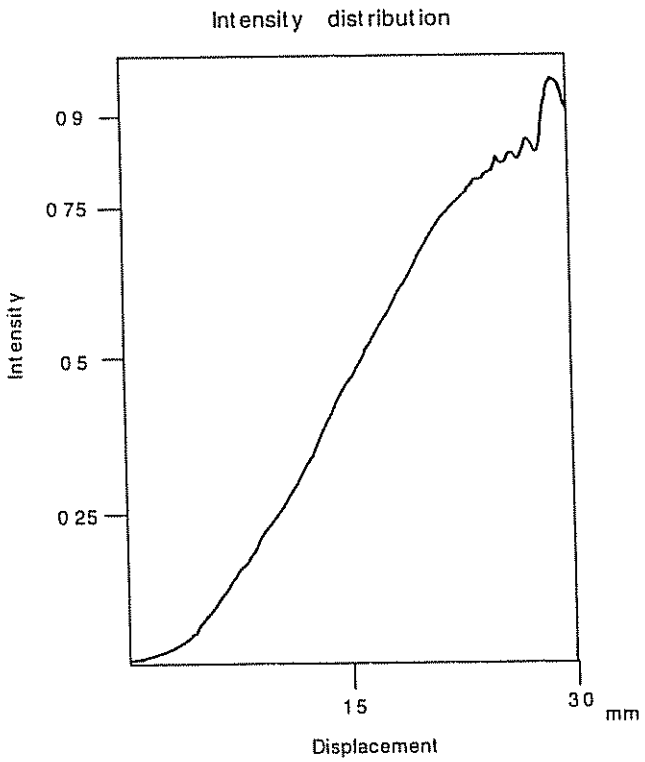

Fig. 14 Measured intensity distribution along the line at the focus plane.

The maximal normalized power at the edge of the element was 0.89, which is only 0.08 less than predicted. This reduction is attributed to lithographic errors such as misalignment of the masks and etch depth errors. The deviations from linearity are caused by local scattering and nonuniformities in the DOE, which were averaged and smoothened when the entire element was illuminated.

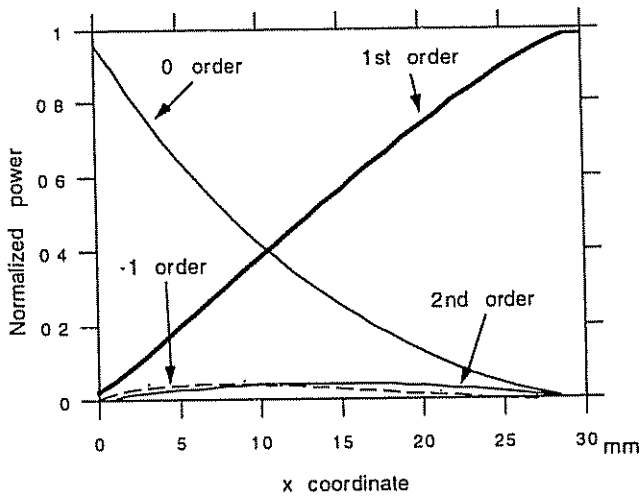

Fig. 15 Predicted power in the diffracted orders as a function of the *y* coordinate of the cylindrical DOE. The power is distributed mainly in the first and second orders.

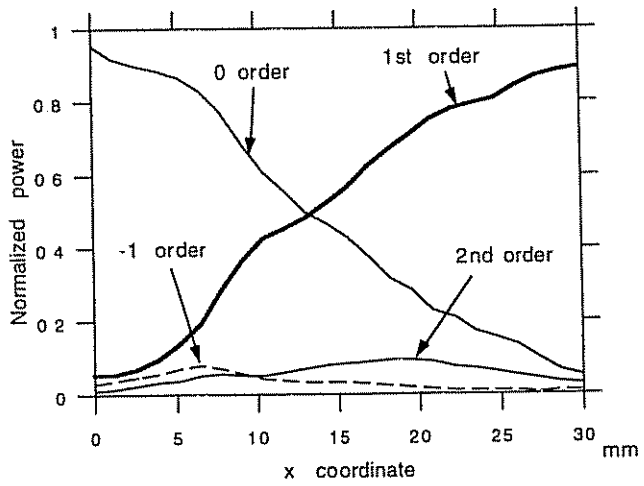

Fig. 16 Measured power in the diffracted orders as a function of the *y* coordinate of the cylindrical DOE.

5 Concluding Remarks

This investigation introduced and evaluated, both with computer simulations and experimentally, a novel design method for optimizing the diffraction efficiency of multilevel DOEs. The optimization was achieved by changing the number and width of the levels in every period of the DOE and by ensuring that the number of levels needed to record the elements is minimized. The result of these investigations can lead to sophisticated and efficient DOEs that could be in incorporated into applications hitherto impossible.

Acknowledgment

This work was supported in part by the Israel Ministry of Sciences and Arts.

References

1. W. H. Lee, "Computer generated holograms: techniques and applications," *Prog. Opt.* **16**, 119–232 (1978).
2. J. A. Jordan, P. M. Hirsch, L. B. Lesem, and D. L. Van Rooy, "Kinoform lenses," IBM Publication 320, 2357–2361 (1969).
3. J. A. Jordan, P. M. Hirsch, L. B. Lesem, and D. L. Van Rooy, "Kinoform lenses," *Appl. Opt.* **9**, 1883–1887 (1970).
4. E. Hasman, N. Davidson, and A. A. Friesem, "Efficient multilevel phase holograms for CO_2 lasers," *Opt. Lett.* **16**, 423–425 (1991).
5. N. Davidson, R. Duer, A. A. Friesem, and E. Hasman, "Blazed holographic gratings for polychromatic and multidirectional incidence light," *J. Opt. Soc. Am. A* **9**, 1196–1199 (1992).
6. J. A. Davis, D. M. Cottrell, C. A. Maley, and M. R. Crivello, "Subdiffraction-limited focusing lens," *Appl. Opt.* **33**, 4128–4131 (1994).
7. D. C. Chu, J. R. Finup, and J. W. Goodman, "Multiemulsion on axis computer generated holograms," *Appl. Opt.* **12**, 1386–1388 (1973).
8. N. Davidson, A. A. Friesem, and E. Hasman, "Optical coordinate transformations," *Appl. Opt.* **31**, 1067–1073 (1992).
9. J. L. Horner and P. D. Gianino, "Phase only matched filtering," *Appl. Opt.* **23**, 812–816 (1984).
10. B. R. Brown and A. W. Lohmann, "Complex spatial filtering with binary masks," *Appl. Opt.* **5**, 967–969 (1966).
11. E. K. Popov, L. V. Tsonev, and E. G. Loen, "Scalar theory of transmission relief gratings," *Opt. Commun.* **80**, 307–311 (1991).
12. E. Hasman and A. A. Friesem, "Analytic optimization for holographic optical elements," *J. Opt. Soc. Am. A* **6**, 62–72 (1989).

Yochay Danziger received the BSc degree in 1991 from the Ben Gurion University, Beer-Sheva, and the MSc degree in 1995 from the Weizmann Institute of Science, Rehovot, Israel, where he is currently pursuing his doctoral research. His research interests include diffractive optical elements, optical resonators, and far-IR applications.

Erez Hasman received the BSc degree in 1981 from the Tel Aviv University, the MSc degree in 1985 from the Technion, Haifa, and the PhD in 1992 from Weizmann Institute of Science, Rehovot, Israel. From 1981 to 1986 he was employed by the government of Israel, Department of Science, Haifa. From 1992 to 1994, he was chief physicist of graphic and recognition product lines with the Optrotech company, performing research and development in the areas of photoploers and imaging systems for printed circuit boards and graphic arts industries. Presently, he is a technology analysis manager at Elop company in Israel and a scientific consultant at Weizmann Institute of Science. His research interests include holography, diffractive optics, optical computing, optical measurement, optical memory, and nonconventional laser resonators.

Asher A. Friesem received BSc and PhD degrees from the University of Michigan in 1958 and 1968, respectively. From 1958 to 1963 he was employed by Bell Aero Systems Company and Bendix Research Laboratories. From 1963 to 1969 he was at the University of Michigan Institute of Science and Technology, conducting investigations in coherent optics, mainly in the areas of optical data processing and holography. From 1969 to 1973 he was principal research engineer in the Electro-Optics Center of Harris, Inc., performing research in the areas of optical memories and displays. In 1973 he joined the staff of the Weizmann Institute of Science, and became a professor of optical sciences in 1977. He is concerned with new holographic concepts and applications, optical image processing, and electro-optic devices. Friesem is a fellow of the OSA and of IEEE, a member of SPIE, a past chairman of the Israel Laser and Electro-Optics Society, and a member of Eta Kappa Nu and Sigma Xi.

Adolf W. Lohmann has taught and conducted research, mainly in optical information processing, at five universities and in industry in Sweden, the United States, and Germany. From 1973 to 1992 he was a professor of applied optics in the physics department of the University in Erlangen. Since his retirement, he has collaborated with colleagues at the Weizmann Institute, at Tel Aviv University, at the University of Valencia in Spain, and at two Mexican universities: Inaoe and Udla.